Structure of Human Epoxide Hydrolase Reveals Mechanistic Inferences on Bifunctional Catalysis in Epoxide and Phosphate Ester Hydrolysis[†,‡]

German A. Gomez,[§] Christophe Morisseau,[||] Bruce D. Hammock,[||] and David W. Christianson*[,§]

Roy and Diana Vagelos Laboratories, Department of Chemistry, University of Pennsylvania, Philadelphia, Pennsylvania 19104-6323, and Department of Entomology and UCD Cancer Center, University of California, Davis, California 95616-8584

Received December 5, 2003; Revised Manuscript Received February 4, 2004

ABSTRACT: The X-ray crystal structure of human soluble epoxide hydrolase (sEH) has been determined at 2.6 Å resolution, revealing a domain-swapped quaternary structure identical to that observed for the murine enzyme [Argiriadi, M. A., Morisseau, C., Hammock, B. D., and Christianson, D. W. (1999) *Proc. Natl. Acad. Sci. U.S.A. 96,* 10637−10642]. As with the murine enzyme, the epoxide hydrolytic mechanism of the human enzyme proceeds through an alkyl-enzyme intermediate with Asp-333 in the C-terminal domain. The structure of the human sEH complex with *N*-cyclohexyl-*N*′-(iodophenyl)urea (CIU) has been determined at 2.35 Å resolution. Tyr-381 and Tyr-465 donate hydrogen bonds to the alkylurea carbonyl group of CIU, consistent with the proposed roles of these residues as proton donors in the first step of catalysis. The N-terminal domain of mammalian sEH contains a 15 Å deep cleft, but its biological function is unclear. Recent experiments demonstrate that the N-terminal domain of human sEH catalyzes the metal-dependent hydrolysis of phosphate esters [Cronin, A., Mowbray, S., Dürk, H., Homburg, S., Fleming, I., Fisslthaler, B., Oesch, F., and Arand, M. (2003) *Proc. Natl. Acad. Sci. U.S.A. 100,* 1552−1557; Newman, J. W., Morisseau, C., Harris, T. R., and Hammock, B. D. (2003) *Proc. Natl. Acad. Sci. U.S.A. 100,* 1558−1563]. The binding of Mg^{2+}-HPO_4^{2-} to the N-terminal domain of human sEH in its CIU complex reveals structural features relevant to those of the enzyme−substrate complex in the phosphatase reaction.

Two distinct forms of epoxide hydrolase, microsomal and soluble, are found in the mammalian liver, and each catalyzes a hydrolytic epoxide ring opening reaction to yield a vicinal diol product. The microsomal enzyme hydrolyzes xenobiotic toxins, such as oxidized metabolites of polycyclic aromatic hydrocarbons and other epoxides capable of alkylating proteins and nucleic acids (*1*). Soluble epoxide hydrolase (sEH)[1] plays a broader role in biology by virtue of its activity against lipid epoxide substrates and its localization not only in liver but also in kidneys and vascular tissue (*2, 3*). The sEH enzyme catalyzes the hydrolysis of *cis*-epoxyeicosatrienoic acids (*4*), which act at vascular, renal, and cardiac levels of blood pressure regulation (*5*). As such, sEH may be a target for the treatment of hypertension (*2*−*4*). Additionally, that sEH catalyzes the hydrolysis of leukotoxin and isoleukotoxin suggests that sEH is a possible target for the treatment of acute respiratory distress syndrome, since the corresponding diols of these epoxides are implicated in the inflammatory cascade (*6*).

The 2.8 Å resolution crystal structure of murine sEH (125 kDa) reveals a homodimeric, domain-swapped architecture in which the C-terminal domain adopts an α/β fold homologous to that of haloalkane dehalogenase (*7*). Extensive enzymological and structural studies demonstrate that epoxide substrates bind in a 25 Å long, "L"-shaped hydrophobic tunnel in the C-terminal domain: epoxide ring opening is facilitated by general acid catalysts Tyr-381 and Tyr-465, with concomitant nucleophilic attack by Asp-333 to form an alkylenzyme intermediate (*7*−*15*). Intriguingly, the N-terminal domain adopts an α/β fold homologous to that of haloacid dehalogenase and contains a 15 Å deep cleft. The N-terminal domain does not participate in epoxide hydrolysis, since competitive inhibitors of the epoxide hydrolysis reaction bind exclusively to the C-terminal domain (*7*−*9*). At the very least, the N-terminal domain plays an important role in the stabilization of the domain-swapped quaternary structure (*7*). Given its structural similarity and low but measurable amino acid sequence identity with phosphonoacetaldehyde hydrolase (15%), as well as the conservation of active site residues between these two enzymes (*16*), could the N-terminal domain of mammalian sEH similarly function as a metal-dependent phosphatase?

A potential clue as to the function of the N-terminal domain of sEH emanated from the initial structure determination of the enzyme, in which the samarium acetate derivative used for phasing revealed a single Sm^{3+} binding site at the base of the cleft in the N-terminal domain (*7*, *17*). Since Sm^{3+} can bind to catalytic Mg^{2+} sites in metal-requiring enzymes [e.g., farnesyl diphosphate synthase (*18*)

[†] Funding was provided by NIH Research Grant GM63106 (D.W.C.), NIEHS Grant R37 ES02710, and NIEHS Superfund Basic Research Program Grant P42 ES04699 (B.D.H.).

[‡] Coordinates of human sEH and the human sEH−CIU complex have been deposited in the Protein Data Bank with accession codes 1S8O and 1VJ5, respectively.

* To whom correspondence should be addressed. Tel: 215-898-5714. Fax: 215-573-2201. E-mail: chris@xtal.chem.upenn.edu.

[§] University of Pennsylvania.

[||] University of California, Davis.

[1] Abbreviations: sEH, soluble epoxide hydrolase; DTT, dithiothreitol; CIU, *N*-cyclohexyl-*N*′-(iodophenyl)urea; PHO, phosphonoxyhydroxyoctadecanoic acid.

10.1021/bi036189j CCC: $27.50
Published on Web 04/02/2004

and aristolochene synthase (*19*)] and since Sm^{3+}-binding residues in sEH are conserved as Mg^{2+}-binding residues in phosphonacetaldehyde hydrolase (*16*, *17*), we hypothesized that the N-terminal domain of sEH might exhibit a Mg^{2+}-dependent hydrolytic function. Accordingly, reports that the N-terminal domain of sEH catalyzes the Mg^{2+}-dependent hydrolysis of phosphate esters (D. Dunaway-Mariano, personal communication, Sept 1, 1999; *20*, *21*) confirm that this domain is an enzyme unto itself with structure−activity relationships distinct from those of the C-terminal epoxide hydrolase domain.

To clarify structure−mechanism relationships in the bifunctional mammalian sEH enzymes, we now report the 2.6 Å resolution structure of native human sEH and its complex with the inhibitor *N*-cyclohexyl-*N*′-(iodophenyl)urea (CIU) at 2.35 Å resolution. Importantly, Mg^{2+}-HPO_4^{2-} binds in the active site cleft of the N-terminal phosphatase domain in the sEH−inhibitor complex, so this structure reveals important clues on the function of Mg^{2+} and neighboring protein residues in the hydrolysis of phosphate ester substrates.

MATERIALS AND METHODS

Recombinant human sEH was produced in a baculovirus expression system and purified as described (*22*, *23*), with the addition of a final step using a Superdex 200 (Amersham Pharmacia) size exclusion column in 0.1 M sodium phosphate and 3 mM dithiothreitol (DTT) (pH 7.4). For crystallization by vapor diffusion, a sitting drop containing 5.0 μL of protein solution [12−16 mg/mL sEH, 3 mM DTT, 0.1 M sodium phosphate (pH 7.4)] and 5.0 μL of precipitant buffer [0.1 M Tris (pH 9.0), 30% (w/v) PEG 4000, and 0.2 M Li_2SO_4] was equilibrated with a 1 mL reservoir of precipitant buffer at 4 °C. Rodlike crystals appeared in approximately 10 days with dimensions of 0.3 mm × 0.2 mm × 1 mm. Following transfer to a 20% sucrose cryoprotectant and flash cooling, crystals yielded diffraction data to 2.6 Å resolution at the Cornell High Energy Synchrotron Source (beamline F-1 with an ADSC Quantum 4 detector at 100 K). Crystals belonged to space group $P6_522$ with unit cell parameters $a = b = 92.6$ Å and $c = 244.6$ Å. With one monomer in the asymmetric unit, $V_m = 2.4$ Å^3/Da, corresponding to 48% solvent content.

The preparation of the human sEH−CIU complex was achieved by crystal soaking experiments. First, the native enzyme was crystallized in a sitting drop containing 5.0 μL of protein solution [12−16 mg/mL sEH, 3 mM DTT, 0.1 M sodium phosphate (pH 7.4)], 5.0 μL of a modified precipitant buffer [0.1 M Tris (pH 8.4), 34% (w/v) PEG 3350], and 0.5 μL *n*-hexadecyl β-D-maltoside (Hampton), equilibrated against a 1 mL reservoir of modified precipitant buffer at 4 °C. Hexagonal rods appeared in approximately 7 days with dimensions of 0.3 mm × 0.3 mm × 1 mm. Crystals were then soaked in the modified precipitation buffer augmented with 5 mM CIU for 10 days. Following transfer to a 20% sucrose cryoprotectant solution and flash cooling, crystals of the human sEH−CIU complex yielded diffraction data to 2.35 Å resolution at the Advanced Light Source, Berkeley (beamline BL 5.0.1 with an ADSC Quantum 4U detector at 100 K), and belonged to space group $P6_522$ with unit cell parameters $a = b = 93.5$ Å and $c = 245.7$ Å.

Data reduction was achieved with Denzo and Scalepack (*24*). Molecular replacement calculations utilized AMORE (*25*) with the native murine sEH B monomer (1CQZ) (*7*) as the search probe. Iterative cycles of refinement and model building using CNS (*26*) and O (*27*), respectively, improved each protein structure as monitored by R_{free}. Group *B*-factors were utilized during refinement. Buffer molecules, ions, and water molecules were included in later cycles of refinement. Notably, an electron density peak in the N-terminal domain active site was interpreted as Mg^{2+} and refined with a *B*-factor of 22 Å^2, consistent with the average *B*-factor of 30 Å^2 for the entire protein. Refinement of this peak as Li^+ or Ca^{2+} yielded anomalously low or high *B*-factors, respectively. Data reduction and refinement statistics are recorded in Table 1.

Table 1: Data Collection and Refinement Statistics

structure	human sEH	human sEH−CIU complex
limiting resolution, Å	2.6	2.35
R_{merge}[a]	0.100	0.127
$I/\sigma I$	30.9	21.5
no. of reflections, work/test	18072/1544	24669/2711
R/R_{free}[b]	0.216/0.272	0.217/0.266
protein atoms[c]	4320	4331
water molecules[c]	39	228
metal ions/ligand atoms[b]	0/0	1/22
rms deviations		
bond lengths, Å	0.007	0.006
bond angles, deg	2.0	1.3
dihedral angles, deg	22.8	22.5
improper dihedral angles, deg	1.1	0.8

[a] $R_{merge} = \sum|I - \langle I\rangle|/\sum I$, where I is the observed intensity and $\langle I\rangle$ is the average intensity calculated for replicate data. [b] Crystallographic *R*-factor, $R = \sum|F_o| - |F_c|/\sum|F_o|$, for reflections contained in the working set. Free *R*-factor, $R_{free} = \sum|F_o| - |F_c|/\sum|F_o|$, for reflections contained in the test set excluded from refinement (8% of total). $|F_o|$ and $|F_c|$ are the observed and calculated structure factor amplitudes, respectively. [c] Per asymmetric unit.

Disordered segments at the N- and C-termini (native sEH, Met-1−Leu-3 and Pro-548−Met-554; sEH−CIU complex, Met-1 and Pro-548−Met-554) were absent in the experimental electron density and were not included in the final models. Only one residue in each final model, Asn-357, exhibited a disallowed backbone conformation. Asn-357 appears in a well-ordered region of electron density, and its side chain hydrogen bonds with Asp-495 and Thr-525. The atomic coordinates of human sEH and its CIU complex have been deposited in the PDB with accession codes 1S8O and 1VJ5, respectively. Figures were prepared with MOLSCRIPT2 (*28*), BOBSCRIPT with Raster3D (*29*, *30*), and AVS (*31*).

RESULTS AND DISCUSSION

Human sEH Structure and Mechanism of Epoxide Hydrolysis. The amino acid sequences of murine sEH and human sEH are 73% identical. Accordingly, it is not surprising that the overall tertiary and quaternary structures are similar. Human sEH exhibits a domain-swapped architecture identical to that of murine sEH (*7*) (Figure 1). However, the two domains in each subunit shift away from each other by ~4 Å about a hinge approximately defined by the proline-rich linker segment (Thr-219−Asp-234 in murine sEH and Ile-219−Asp-234 in human sEH).[2] This contributes to the rms deviation of 1.4 Å measured for the 505 Cα atoms common to human and murine sEH monomers.

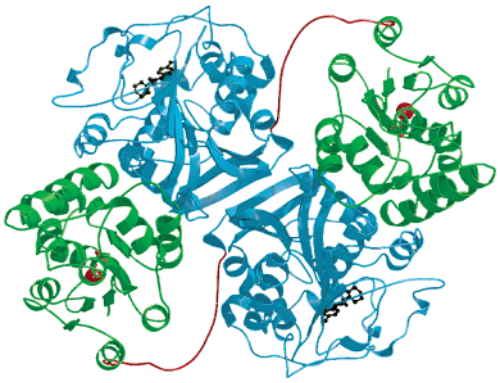

FIGURE 1: Structure of the human sEH dimer. The N-terminal domains are in green, the C-terminal domains are in blue, and the proline-rich linker segment (Ile-219−Asp-234) is in red. The inhibitor CIU (black stick figure) is bound in the epoxide hydrolase active site, and Mg^{2+}-HPO_4^{2-} (red sphere and stick figure) is bound in the phosphatase active site.

Some differences in tertiary structure are evident between the individual domains of human sEH and murine sEH. Superposition of the N-terminal domains yields an rms deviation of 1.8 Å for 210 Cα atoms (Figure 2), while superposition of the C-terminal domains yields an rms deviation of 0.5 Å for 300 Cα atoms (Figure 3). Significant structural differences are mostly confined to loop segments of the structure, and in human sEH these segments are characterized by distinctly high thermal *B*-factors, which may reflect some disorder. Human segment Ala-40−Glu-57 contains a short α-helical segment, whereas Ala-40−Lys-57 of murine sEH adopts a random coil conformation.

As in the murine enzyme, the active site for epoxide hydrolysis in human sEH lies in an ∼25 Å long, L-shaped hydrophobic tunnel in the C-terminal domain. Interestingly, the active site for expoxide hydrolysis is occupied by an unidentified ligand (data not shown). However, the electron density corresponding to this ligand is not interpretable as a buffer molecule (Tris) nor is it interpretable as any other component of the buffer solution. The catalytic nucleophile, Asp-333, is located at the "bend" in the L-shaped tunnel. The carboxylate side chain of Asp-333 is oriented by hydrogen bond interactions with His-523 and the backbone NH groups of Phe-265 and Trp-334. The imidazole ring of His-523 is oriented by a hydrogen bond interaction with the carboxylate side chain of Asp-495. Directly across from Asp-333 are the phenolic side chains of Tyr-381 and Tyr-465, situated favorably to act as general acid catalysts to accelerate epoxide ring opening (*8*, *9*). This active site structure is consistent with the S_N2-type mechanism outlined for murine sEH (*7*−*11*, *32*): Asp-333 attacks the epoxide substrate to form an alkyl-enzyme intermediate, subsequently hydrolyzed by a water molecule (assisted by general base His-523) to yield the diol product.

Binding of an Alkylurea Inhibitor. Despite the high degree of sequence and structural similarity between murine sEH and human sEH and despite roughly comparable enzyme−inhibitor affinities, significant differences are observed in the binding of the inhibitor CIU to each enzyme. For reference, CIU binding to human sEH and murine sEH yields IC_{50} values of 0.12 and 0.07 μM, respectively (*33*, *34*).

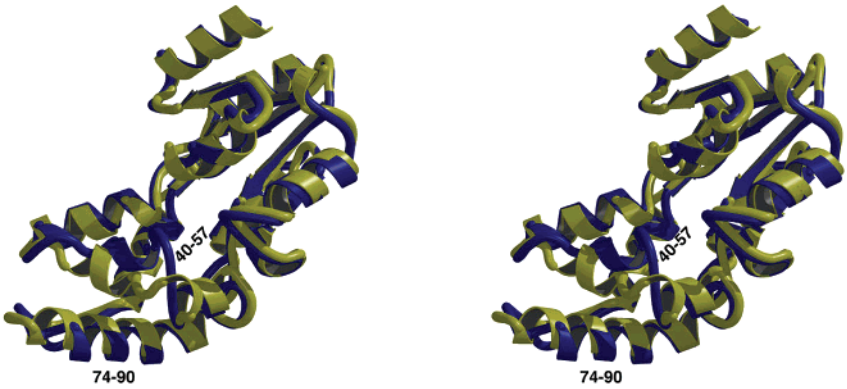

FIGURE 2: Superposition of the human sEH N-terminal domain (yellow) and the murine sEH N-terminal domain (blue). Amino acid segments exhibiting structural differences between human and murine enzymes are indicated by sequence numbers.

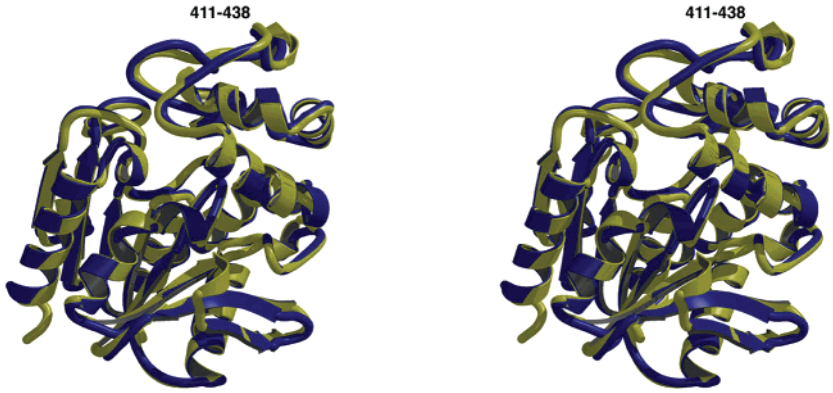

FIGURE 3: Superposition of the human sEH C-terminal domain (yellow) and the murine sEH C-terminal domain (blue). Amino acid segments exhibiting structural differences between human and murine enzymes are indicated by sequence numbers.

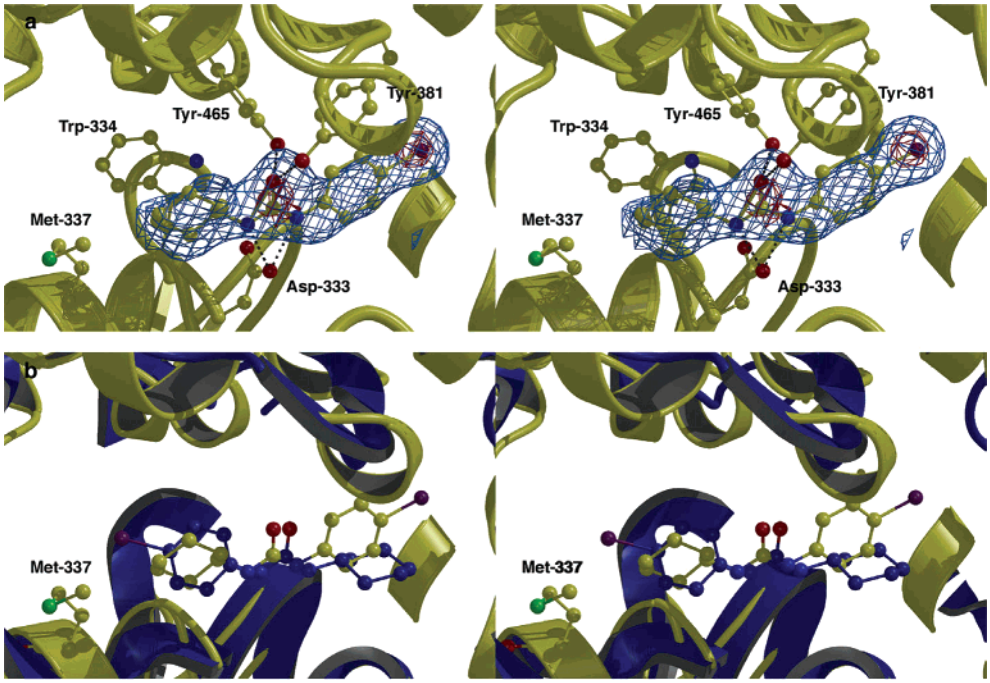

FIGURE 4: (a) Omit electron density map [contoured at 3.5σ (cyan) and 10σ (red)] of the complex between human sEH and *N*-cyclohexyl-*N*′-(iodophenyl)urea (CIU). The position of the electron-rich iodine atom of CIU is clearly indicated by the 10σ contour (red). Selected active site residues are indicated, and hydrogen bond interactions are depicted as dashed lines. (b) Superposition of the human sEH−CIU complex (yellow) and the murine sEH−CIU complex (blue). Note that CIU binds with opposite orientations to the human and murine enzymes.

The binding of CIU to the C-terminal domain of human sEH triggers no major conformational changes, and the rms deviation of 541 Cα atoms between the native and CIU-complexed enzymes is 0.4 Å. The binding of CIU is stabilized by hydrogen bond interactions between the urea oxygen and Tyr-381 and Tyr-465 and between the urea NH groups and Asp-333. Unambiguous assignment of the inhibitor orientation is made by clear placement of the electron-rich iodophenyl substituent (Figure 4a). The *N*-cyclohexyl group of CIU makes van der Waals interactions with Trp-334, Met-337, and Leu-498, and the *N*′-iodophenyl substituent makes van der Waals interactions with Phe-265, Tyr-381, Leu-406, Val-497, and Trp-524.

Superposition of the murine and human sEH−CIU complexes reveals that CIU binds with opposite orientations in the active sites of each enzyme (Figure 4b). The reversed binding mode of CIU to human sEH can be attributed to the steric bulk of Met-337 in comparison with Val-337 of murine sEH: Met-337 of human sEH constricts one side of the active site tunnel and precludes the binding of the bulky iodophenyl substituent of CIU with the orientation observed in the murine sEH−CIU complex. This finding agrees with a recent QSAR study of sEH inhibition by alkylureas, including CIU (*35*). Specifically, a steric parameter is important for describing the potency of inhibitors against murine sEH but not against human sEH. If all of the compounds studied by Morrisseau and colleagues (*35*) are oriented like CIU, para-substituted groups such as the iodophenyl group of CIU are located in the less constricted side of the active pocket and do not encounter any steric limitation. Intriguingly, a QSAR study of the binding of chalcone oxides to human sEH (*36*) did not yield a satisfactory Hansch equation. The binding of some derivatives in one orientation and others in the opposite orientation could explain the difficulty in finding a structure−activity correlation, and this phenomenon could complicate QSAR studies of some, but not necessarily all, classes of inhibitors.

Structural Aspects of Catalysis by the N-Terminal Domain of sEH. A phosphatase-like active site in the N-terminal domain of sEH was suggested by structural comparison of murine sEH (*7*) and phosphonoacetaldehyde hydrolase (*16*) (K. Allen and M. A. Argiriadi, personal communications, Aug 5, 1999), in that Sm^{3+} interacts with residues in the N-terminal domain of sEH that are conserved in phosphatases and phosphonatases: Asp-9, Asp-11, Asp-184, and Asp-185 (data not shown) (*16*). Since Sm^{3+} is a Mg^{2+} analogue, this result suggested a potentially functional Mg^{2+} site in sEH. Demonstration of the Mg^{2+}-dependent hydrolysis of *p*-nitrophenyl phosphate indicated a phosphatase-like function for the N-terminal domain of murine sEH (D. Dunaway-Mariano, personal communication, Sept 1, 1999), and this has been subsequently demonstrated for both murine sEH and human sEH (*20*, *21*). Specifically, Newman and colleagues (*20*) report that a single Mg^{2+} ion binds to each sEH monomer with micromolar affinity, and Cronin and colleagues (*21*) show that a construct consisting of solely the N-terminal domain of human sEH exhibits Mg^{2+}-dependent phosphatase activity nearly identical to that measured for the full-length enzyme.

The crystal structure of the human sEH−CIU complex profoundly illuminates this novel aspect of phophatase-like catalysis and reveals the binding of a metal ion interpreted as Mg^{2+} to the N-terminal domain[3] in a location essentially identical to that observed for Sm^{3+} binding to the murine

[2] The numbering scheme established for murine sEH is adapted here for human sEH. Amino acid insertions are designated by a letter suffix following the sequence number of the point of insertion, e.g., Leu-222, Asn-222A, and Thr-222B.

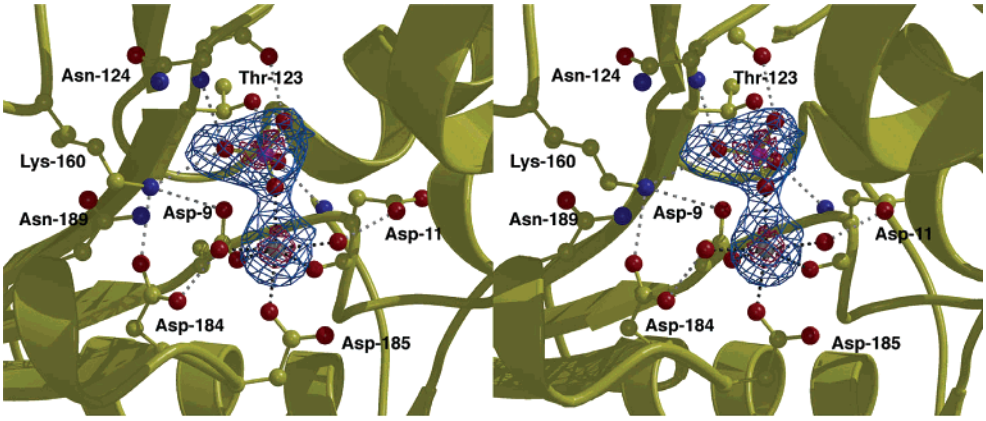

FIGURE 5: Omit electron density map [contoured at 4.0σ (blue) and 9.0σ (pink)] of the Mg^{2+}-HPO_4^{2-} binding site in the human sEH−CIU complex.

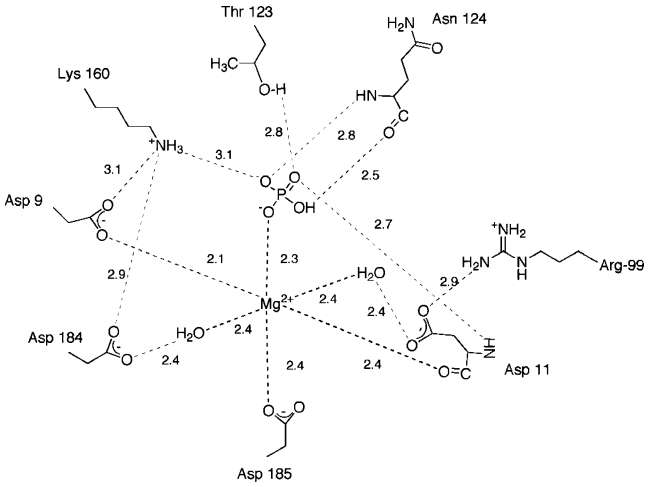

FIGURE 6: Schematic diagram of the Mg^{2+} binding site in the N-terminal domain of the human sEH−CIU complex. Hydrogen bond interactions and metal coordination interactions are depicted as dotted lines, and selected distances are indicated in angstroms.

enzyme. Additionally bound is the HPO_4^{2-} ion from buffer, so the structure of the sEH−Mg^{2+}-HPO_4^{2-} complex mimics that of an actual enzyme−substrate complex for phosphate ester hydrolysis. An electron density map of the phosphatase active site in the human sEH−CIU complex is shown in Figure 5.

The binding of Mg^{2+}-HPO_4^{2-} reveals interactions with several residues that may be important for catalysis in the N-terminal domain (Figures 5 and 6). The Mg^{2+} ion is octahedrally coordinated by Asp-9 (Oδ2), Asp-185 (Oδ1), the backbone carbonyl oxygen of Asp-11, water molecule 779 (which also donates a hydrogen bond to Oδ1 of Asp-184), water molecule 670 (which donates a hydrogen bond to Oδ2 of Asp-11; Oδ2 of Asp-11 accepts a hydrogen bond from Arg-99), and phosphate O1. In addition to the metal coordination interaction via O1, the molecular recognition of the HPO_4^{2-} ion is achieved by an extensive array of hydrogen bond interactions: phosphate O2 accepts hydrogen bonds from Lys-160 and the backbone NH group of Asn-124, phosphate O3 accepts hydrogen bonds from Thr-123 and the backbone NH group of Asp-11, and phosphate O4-H donates a hydrogen bond to the backbone carbonyl oxygen of Asn-124. The phosphate O4-H group is oriented toward the entrance to the active site cleft. Accordingly, the phosphate O4 atom is the likely point of attachment for the alkyl substituent of phosphate ester substrates such as *p*-nitrophenyl phosphate and *threo*-9/10-phosphonoxyhydroxyoctadecanoic acid (*20*, *21*).

Although the Oδ1 atom of Asp-9 is within 2.7−3.2 Å of phosphate oxygens O1, O2, and O3, we do not interpret these interactions as hydrogen bonds. Since the Asp-9 Oδ1 is 3.0 Å from the central phosphorus atom of HPO_4^{2-} and is oriented nearly in-line with the P−O4 bond (Asp-9 Oδ1•• •P−O4 angle = 169°), we interpret the close contact of Asp-9 to reflect its proposed role as a catalytic nucleophile (*21*), for which its negatively charged carboxylate group must approach the negatively charged phosphate group of the substrate. The negative charge of the substrate phosphate group is screened by Mg^{2+} coordination and an extensive array of hydrogen bond interactions to facilitate the interaction of Asp-9 Oδ1 with the electropositive phosphorus atom. This is consistent with the catalytic strategy deduced in structural and mechanistic studies of the related enzyme phosphonatase (*16*, *37*, *38*). In human sEH, it is notable that the Asp-9 → Ala variant exhibits no phosphatase activity, consistent with the critical role of this residue as a catalytic nucleophile (*21*) and Mg^{2+} ligand.

The active site cleft in the N-terminal domain assumes the shape of a "mitt" or hand with the magnesium binding site located at the bottom of an ~15 Å deep negatively charged pocket. This pocket is situated along a 25 Å long hydrophobic cleft formed as residues Leu-16−Lys-100 pack against the core of the N-terminal domain. A model of the substrate *threo*-9/10-phosphonoxyhydroxyoctadecanoic acid (PHO) (*20*) docked into the cleft highlights an extensive hydrophobic surface that can interact with hydrophobic substrates, largely comprised of residues Ala-18, Val-19, Phe-20, Phe-41, Met-54, Pro-161, Pro-46, and Ile-186 (Figure 7). Only Met-54, Pro-161, and Pro-46 are conserved in murine sEH. An unexpected feature of the N-terminal domain active site is an ~14 Å long hydrophobic tunnel sufficiently large to accommodate the binding of an aliphatic substrate (Figure 7), the other end of which is near the interface of the N- and C-terminal domains. Residues lining this tunnel include Val-19, Ser-125, Leu-10, Trp-126, Leu-136, Met-140, and Arg-99; all except Val-19 and Ser-125 are conserved in murine sEH, possibly suggestive of a conserved

[3] The electron density in the N-terminal domain of the human sEH−inhibitor complex is consistent with the binding of Mg^{2+} encountered as a trace contaminant in the crystallization reagents.

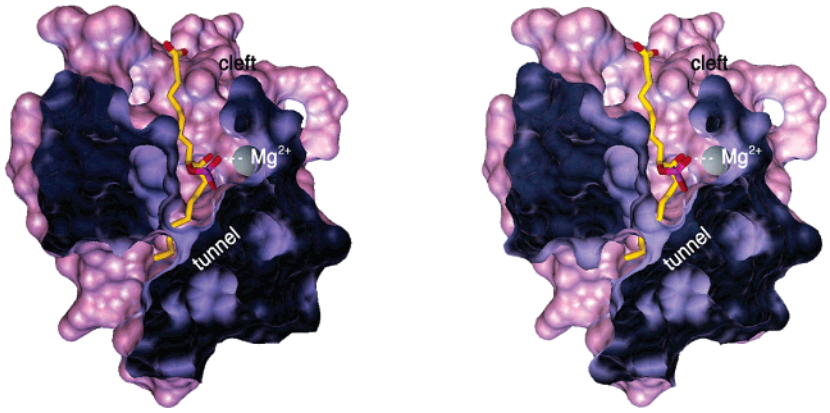

FIGURE 7: Model of substrate phosphonoxyhydroxyoctadecanoic acid (PHO) binding in the phosphatase active site in the N-terminal domain. The hydrophobic tunnel may accommodate the binding of an aliphatic substrate. The molecule is sliced open to better view the hydrophobic tunnel.

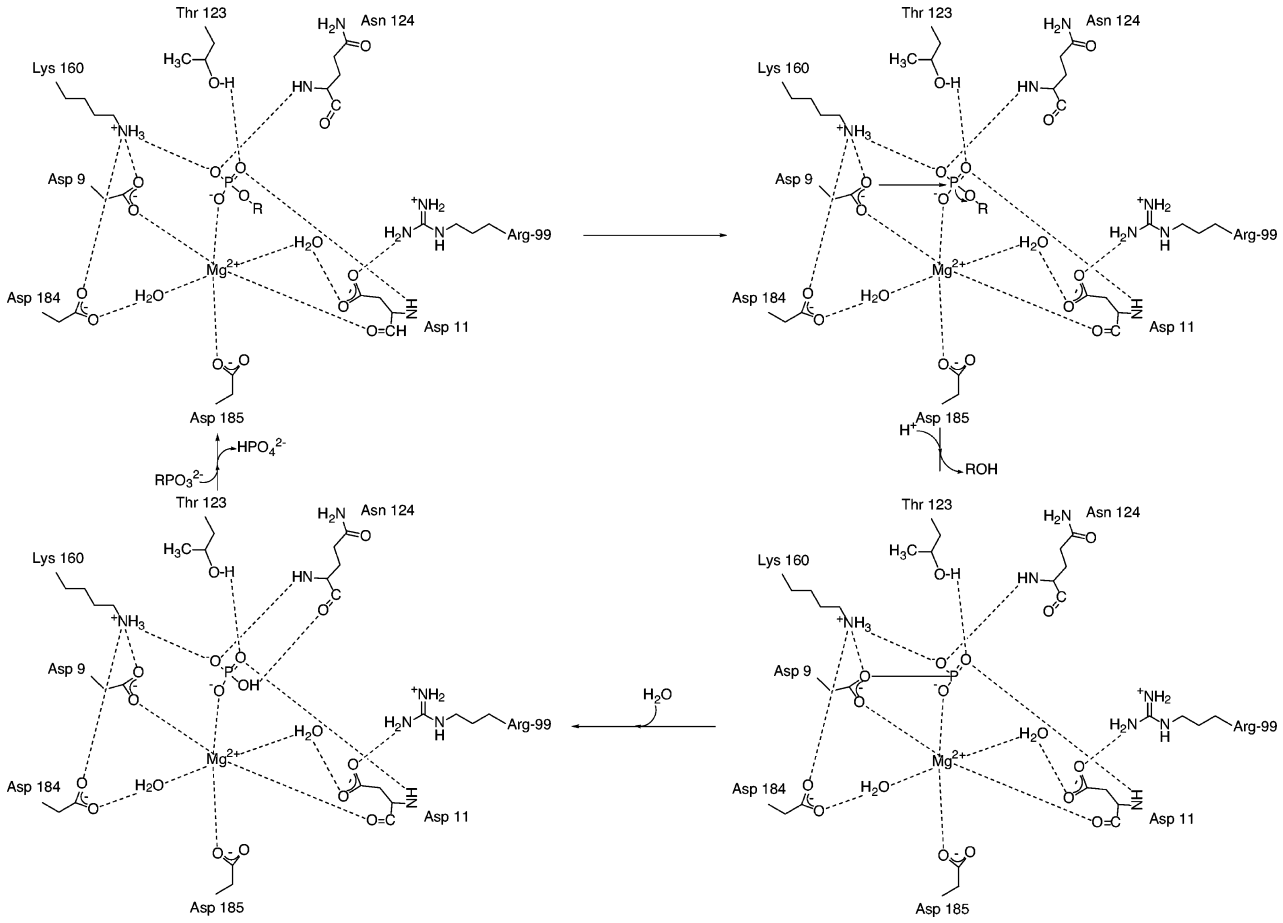

FIGURE 8: Mechanistic proposal for the phosphate ester hydrolysis reaction catalyzed by the N-terminal domain of sEH.

function. Clearly, future site-directed mutagenesis experiments are required to probe the catalytic importance of this tunnel for the sEH-catalyzed phosphatase reaction.

The structure of the human sEH−Mg^{2+}-HPO_4^{2-} complex interpreted in light of enzymological studies of the sEH-catalyzed phosphatase reaction (*20*, *21*), as well as structural and enzymological studies of homologous phosphonatases (*16*, *37*, *38*) and phosphatases (*39*−*41*), leads to a mechanistic proposal for the phosphate ester hydrolysis reaction involving a covalent phosphoenzyme intermediate with Asp-9 (Figure 8). Briefly, the molecular recognition of the anionic substrate phosphoester group by Mg^{2+} coordination and an extensive array of hydrogen bond interactions position the phosphoester for nucleophilic attack by Asp-9. Proton donation to the hydroxyl leaving group may be achieved by the carboxylic acid side chain of Asp-11 or an intervening water molecule, presuming that Asp-11 can break its hydrogen bond with Arg-99 and undergo a substrate-induced conformational change as observed for the corresponding residue in the homologous enzyme β-phosphoglucomutase (*42*, *43*). The resulting phosphoenzyme intermediate is hydrolyzed either by nucleophilic attack of Mg^{2+}-activated water at the Asp-9 carbonyl or, instead, by in-line nucleophilic attack of a water molecule at the phosphorus atom. In-line nucleophilic attack of the phosphoenzyme intermediate occurs in phosphonatase (*38*), whereas nucleophilic attack

at the carbonyl of the alkyl-enzyme intermediate is established for haloacid dehalogenase (*44*). Either hydrolytic pathway would yield a Mg^{2+}-HPO_4^{2-} product complex identical to that seen in the human sEH−CIU complex. Future enzymological experiments will allow us to pinpoint the mechanistic details of catalysis by the N-terminal phosphatase domain of sEH.

ACKNOWLEDGMENT

We thank Karen Allen, Maria Argiriadi, Debra Dunaway-Mariano, and John Newman for numerous scientific discussions. This work is based on research conducted at the Cornell High Energy Synchrotron Source (CHESS) and the Advanced Light Source at Berkeley (ALS).

REFERENCES

1. Hammock, B. D., Grant, D., and Storms, D. (1997) *Epoxide hydrolases*, *Comprehensive Toxicology* (Sipes, I., McQueen, C., and Gandolfi, A., Eds.) Vol. 3, pp 283−305, Pergamon, Oxford.
2. Imig, J. D., Zhao, X., Capdevila, J. H., Morisseau, C., and Hammock, B. D. (2002) Soluble epoxide hydrolase inhibition lowers arterial blood pressure in angiotensin II hypertension, *Hypertension 39*, 690−694.
3. Fang, X., Kaduce, T. L., Weintraub, N. L., Harmon, S., Teesch, L. M., Morisseau, C., Thompson, D. A., Hammock, B. D., and Spector, A. A. (2001) Pathways of epoxyeicosatrienoic acid metabolism in endothelial cells, *J. Biol. Chem. 276*, 14867−14874.
4. Zeldin, D. C., Kobayashi, J., Falck, J. R., Winder, B. S., Hammock, B. D., Snapper, J. R., and Capdevila, J. H. (1993) Regio- and enantiofacial selectivity of epoxyeicosatrienoic acid hydration by cytosolic epoxide hydrolase, *J. Biol. Chem. 268*, 6402−6407.
5. Fleming, I. (2001) Cytochrome P450 enzymes in vascular homeostasis, *Circ. Res. 89*, 753−762.
6. Moghaddam, M. F., Grant, D. F., Cheek, J. M., Greene, J. F., Williamson, K. C., and Hammock, B. D. (1997) Bioactivation of leukotoxins to their toxic diols by epoxide hydrolase, *Nat. Med. 3*, 562−566.
7. Argiriadi, M. A., Morisseau, C., Hammock, B. D., and Christianson, D. W. (1999) Detoxification of environmental mutagens and carcinogens: structure, mechanism, and evolution of liver epoxide hydrolase, *Proc. Natl. Acad. Sci. U.S.A. 96*, 10637−10642.
8. Yamada, T., Morisseau, C., Maxwell, J. E., Argiriadi, M. A., Christianson, D. W., and Hammock, B. D. (2000) Biochemical evidence for the involvement of tyrosine in epoxide activation during the catalytic cycle of epoxide hydrolase, *J. Biol. Chem. 275*, 23082−23088.
9. Argiriadi, M. A., Morisseau, C., Goodrow, M. H., Dowdy, D. L., Hammock, B. D., and Christianson, D. W. (2000) Binding of alkylurea inhibitors to epoxide hydrolase implicates active site tyrosines in substrate activation, *J. Biol. Chem. 275*, 15265−15270.
10. Borhan, B., Jones, A. D., Pinot, F., Grant, D. F., Kurth, M. J., and Hammock, B. D. (1995) Mechanism of soluble epoxide hydrolase, *J. Biol. Chem. 270*, 26923−26930.
11. Arand, M., Wagner, H., and Oesch, F. (1996) Asp333, Asp495, and His523 form the catalytic triad of rat soluble epoxide hydrolase, *J. Biol. Chem. 271*, 4223−4229.
12. Hammock, B. D., Pinot, F., Beetham, J. K., Grant, D. F., Arand, M. E., and Oesch, F. (1994) Isolation of a putative hydroxyacyl enzyme intermediate of an epoxide hydrolase, *Biochem. Biophys. Res. Commun. 198*, 850−856.
13. Lacourciere, G. M., and Armstrong, R. N. (1993) The catalytic mechanism of microsomal epoxide hydrolase involves an ester intermediate, *J. Am. Chem. Soc. 115*, 10466−10467.
14. Müller, F., Arand, M., Frank, H., Seidel, A., Hinz, W., Winkler, L., Hänel, K., Blée, E., Beetham, J. K., Hammock, B. D., and Oesch, F. (1997) Visualization of a covalent intermediate between microsomal epoxide hydrolase, but not cholesterol epoxide hydrolase, and their substrates, *Eur. J. Biochem. 245*, 490−496.
15. Laughlin, L. T., Tzeng, H.-F., Lin, S., and Armstrong, R. N. (1998) Mechanism of microsomal epoxide hydrolase. Semifunctional site-specific mutants affecting the alkylation half-reaction, *Biochemistry 37*, 2897−2904.
16. Morais, M. C., Zhang, W., Baker, A. S., Zhang, G., Dunaway-Mariano, D., and Allen, K. N. (2000) The crystal structure of *Bacillus cereus* phosphonoacetaldehyde hydrolase: insight into catalysis of phosphorus bond cleavage and catalytic diversification within the HAD enzyme superfamily, *Biochemistry 39*, 10385−10396.
17. Argiriadi, M. (1999) Structure-based mechanism and evolution of liver epoxide hydrolase, Ph.D. Thesis, University of Pennsylvania, Philadelphia, PA.
18. Tarshis, L. C., Yan, M., Poulter, C. D., and Sacchettini, J. C. (1994) Crystal structure of recombinant farnesyl diphosphate synthase at 2.6-Å resolution, *Biochemistry 33*, 10871−10877.
19. Caruthers, J. M., Kang, I., Rynkiewicz, M. J., Cane, D. E., and Christianson, D. W. (2000) Crystal structure determination of aristolochene synthase from the blue cheese mold, *Penicillium roqueforti*, *J. Biol. Chem. 275*, 25533−25539.
20. Newman, J. W., Morisseau, C., Harris, T. R., and Hammock, B. D. (2003) The soluble epoxide hydrolase encoded by EPXH2 is a bifunctional enzyme with novel lipid phosphate phosphatase activity, *Proc. Natl. Acad. Sci. U.S.A. 100*, 1558−1563.
21. Cronin, A., Mowbray, S., Dürk, H., Homburg, S., Fleming, I., Fisslthaler, B., Oesch, F., and Arand, M. (2003) The N-terminal domain of mammalian soluble epoxide hydrolase is a phosphatase, *Proc. Natl. Acad. Sci. U.S.A. 100*, 1552−1557.
22. Beetham, J. K., Tian, T., and Hammock, B. D. (1993) cDNA cloning and expression of a soluble epoxide hydrolase from human liver, *Arch. Biochem. Biophys. 305*, 197−201.
23. Wixtrom, R. N., Silva, M. H., and Hammock, B. D. (1988) Affinity purification of cytosolic epoxide hydrolase using derivatized epoxy-activated sepharose gels, *Anal. Biochem. 169*, 71−80.
24. Otwinowski, Z., and Minor, W. (1997) Processing of X-ray diffraction data collected in oscillation mode, *Methods Enzymol. 276*, 307−326.
25. Navaza, J. (1994) *AmoRe*: an automated package for molecular replacement, *Acta Crystallogr. A 50*, 157−163.
26. Brünger, A. T., Adams, P. D., Clore, G. M., DeLano, W. L., Gros, P., Grosse-Kunstleve, R. W., Jiang, J.-S., Kuszewski, J., Nilges, M., Pannu, N. S., Read, R. J., Rice, L. M., Simonson, T., and Warren, G. L. (1998) Crystallography and NMR system: A new software system for macromolecular structure determination, *Acta Crystallogr. D 54*, 905−921.
27. Jones, T. A., Zou, J.-Y., Cowan, S. W., and Kjeldgaard, M. (1991) Improved methods for building protein models in electron density maps and the location of errors in these models, *Acta Crystallogr. A 47*, 110−119.
28. Kraulis, P. J. (1991) *Molscript*: a program to produce both detailed and schematic plots of protein structures, *J. Appl. Crystallogr. 24*, 946−950.
29. Esnouf, R. M. (1997) An extensively modified version of MolScript that includes greatly enhanced coloring capabilities, *J. Mol. Graphics Modell. 15*, 132−134.
30. Merritt, E. A., and Murphy, M. E. P. (1994) *Raster*3D Version 2.0. A program for photorealistic molecular graphics, *Acta Crystallogr. D 50*, 869−873.
31. Upson, C., Faulhaber, T. A., Kamins, D., Laidlaw, D., Schlegel, D., Vroom, J., Gurwitz, R., and van Dam, A. (1989) The application visualization system: a computational environment for scientific visualization, *IEEE Comput. Graphics Appl. 9*, 30−42.
32. Pinot, F., Grant, D. F., Beetham, J. K., Parker, A. G., Borhan, B., Landt, S., Jones, A. D., and Hammock, D. B. (1995) Molecular and biochemical evidence for the involvement of the Asp-333-His-523 pair in the catalytic mechanism of soluble epoxide hydrolase, *J. Biol. Chem. 270*, 7968−7974.
33. Morisseau, C., Goodrow, M. H., Dowdy, D., Zheng, J., Greene, J. F., Sanborn, J. R., and Hammock, B. D. (1999) Potent urea and carbamate inhibitors of soluble epoxide hydrolases, *Proc. Natl. Acad. Sci. U.S.A. 96*, 8849−8854.
34. McElroy, N. R., Jurs, P. C., Morisseau, C., and Hammock, B. D. (2003) QSAR and classification of murine and human soluble epoxide hydrolase inhibition by urea-like compounds, *J. Med. Chem. 46*, 1066−1080.
35. Morisseau, C., Goodrow, M. H., Newman, J. W., Wheelock, C. E, Dowdy, D. L., and Hammock, B. D. (2002) Structural refinement of inhibitors of urea-based soluble epoxide hydrolases, *Biochem. Pharmacol. 63*, 1599−1608.
36. Morisseau, C., Du, G., Newman, J. W., and Hammock, B. D. (1998) Mechanism of mammalian soluble epoxide hydrolase

inhibition by chalcone oxide derivatives, *Arch. Biochem. Biophys. 356*, 214−228.
37. Baker, A. S., Ciocci, M. J., Metcalf, W. W., Kim, J., Babbitt, P. C., Wanner, B. L., Martin, B. M., and Dunaway-Mariano, D. (1998) Insights into the mechanism of catalysis by the P−C bond-cleaving enzyme phosphonoacetaldehyde hydrolase derived from gene sequence analysis and mutagenesis, *Biochemistry 37*, 9305−9315.
38. Lee, S. L., Hepburn, T. W., Swartz, W. H., Ammon, H. L., Mariano, P. S., and Dunaway-Mariano, D. (1992) Stereochemical probe for the mechanism of P−C bond cleavage catalyzed by the *Bacillus cereus* phosphonoacetaldehyde hydrolase, *J. Am. Chem. Soc. 114*, 7346−7354.
39. Qian, N., Stanley, G. A., Hahn-Hagerdal, B., and Radstrom, P. (1994) Purification and characterization of two phosphoglucomutases from *Lactococcus lactis* subsp. *lactis* and their regulation in maltose- and glucose-utilizing cells, *J. Bacteriol. 176*, 5304−5311.
40. Collet, J. F., Gerin, I., Rider, M. H., Veiga-da-Cunha, M., and Van Schaftingen, E. (1997) Human L-3-phosphoserine phosphatase: sequence, expression and evidence for a phosphoenzyme intermediate, *FEBS Lett. 408*, 281−284.
41. Seal, S. N., and Rose, Z. B. (1987) Characterization of a phosphoenzyme intermediate in the reaction of phosphoglycolate phosphatase, *J. Biol. Chem. 262*, 13496−13500.
42. Lahiri, S. D., Zhang, G., Dunaway-Mariano, D., and Allen, K. N. (2003) The pentacovalent phosphorus intermediate of a phosphoryl transfer reaction, *Science 299*, 2067−2071.
43. Lahiri, S. D., Zhang, G., Dunaway-Mariano, D., and Allen, K. N. (2002) Caught in the act: the structure of phosphorylated β-phosphoglucomutase from *Lactococcus lactis*, *Biochemistry 41*, 8351−8359.
44. Liu, J.-Q., Kurihara, T., Miyagi, M., Esaki, N., and Soda, K. (1995) Reaction mechanism of L-2-haloacid dehalogenase of *Pseudomonas* sp. YL. Identification of Asp10 as the active site nucleophile by ^{18}O incorporation experiments, *J. Biol. Chem. 270*, 18309−18312.

BI036189J